Supporting Information for

Kissing-loop nano-kirigami structures with asymmetric transmission and anomalous reflection

Yingying Chen,[1] Qinghua Liang,[1] Haozhe Sun,[1] Xiaochen Zhang,[1] Weikang Dong,[1] Meihua Niu,[1] Yanji Zheng,[1] Yanjie Chen,[2] Cuicui Lu,[1] Lingling Huang,[2] Xiaowei Li,[3] Lan Jiang,[3] Yang Wang, [1,*] and Jiafang Li[1,4,*]

[1]*Key Lab of Advanced Optoelectronic Quantum Architecture and Measurement (Ministry of Education), Beijing Key Lab of Nanophotonics & Ultrafine Optoelectronic Systems, and School of Physics, Beijing Institute of Technology, Beijing 100081, China*

[2]*School of Optics and Photonics, Beijing Institute of Technology, Beijing 100081, China*

[3]*Laser Micro/Nano Fabrication Laboratory, School of Mechanical Engineering, Beijing Institute of Technology, Beijing 100081, China*

[4]*BIT Chongqing Institute of Microelectronics and Microsystem, Chongqing 400000, China*

*Corresponding authors: yangwang@bit.edu.cn, jiafangli@bit.edu.cn

Figure S1

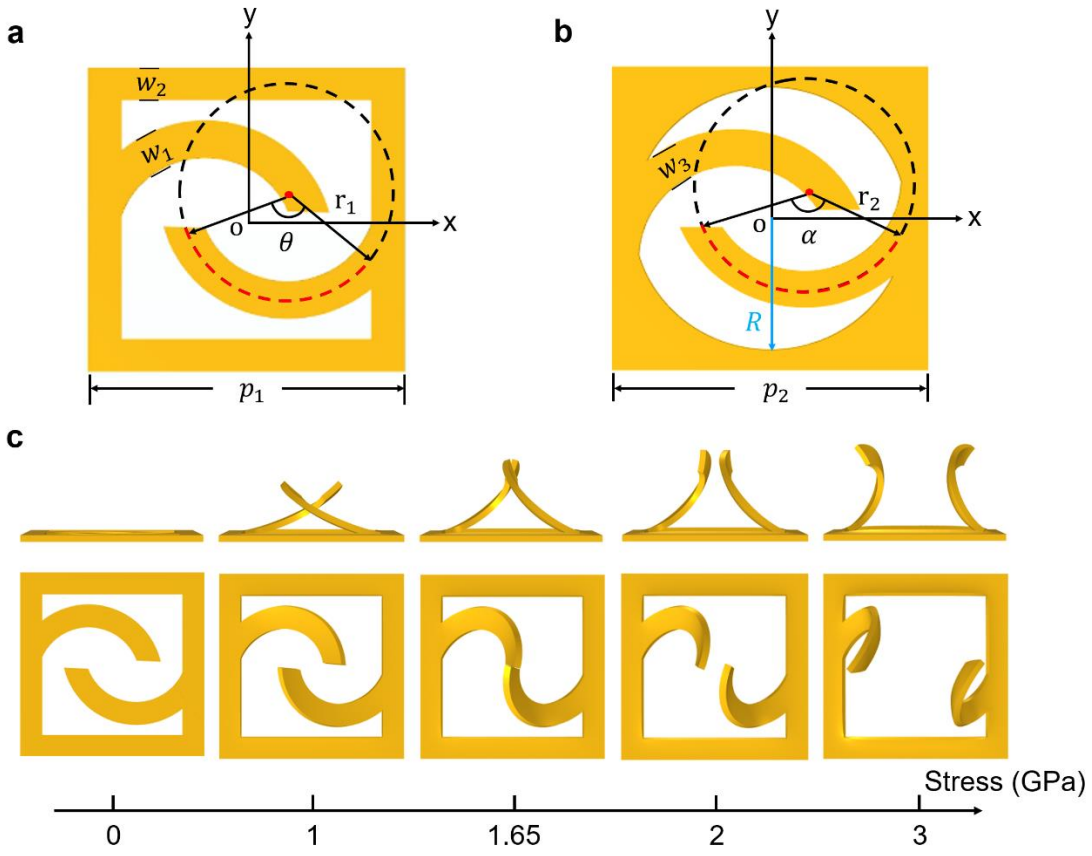

Figure S1. a-b) Detailed parameters of 2D open-loop structures with (a) square and (b) circular supporting frame. a) The period of a unit is $p_1 = 1.7$ μm in x and y direction. It can be seen that the circular supporting frame has more supporting regions. The widths of cantilevers and frame are $w_1 = 0.21$ μm and $w_2 = 0.2$ μm, respectively, while the thickness of gold film is $d = 60$ nm. The curve of cantilever is defined by $x(\theta) = r_1 cos(\theta) + a_1$ and $y(\theta) = r_1 sin(\theta) + b_1$, where the values of r_1, a_1, and b_1 are 0.58, 0.22, 0.13 μm, respectively, and the range of θ is $\theta \in [-167, -40]$. b) The period of a unit is $p_2 = 1$ μm in x and y direction. The width of cantilevers is $w_3 = 0.12$ μm and the thickness of gold film is $d =$ 60 nm. The radius of the inner circle is R = 0.43 μm. The curve of cantilever is defined by $x(\alpha) = r_2 cos(\alpha) + a_2$ and $y(\alpha) = r_2 sin(\alpha) + b_2$, where the values of r_2, a_2, and b_2 are 0.368, 0.108, 0.134 μm, respectively, and the range of θ is $\alpha \in [-155, -25]$. c) The front and top views of two cantilevers deformed under different applied stress. The tips of the two cantilevers are just touched at stress σ =1.65 GPa and $\Delta h = 760$ nm, where the kissing-loop nano-kirigami structures are formed.

Section I. The dynamic process and bilayer stress model of nano-kirigami

The main mechanism of the nano-kirigami is to use the residual stress induced by the gallium ion collisions with gold thin films.[1, 2] Specifically, when the gold nanofilm is irradiated by ion beams, some gold atoms are knocked out and cause surrounding atoms to aggregate towards the vacancies, resulting in tensile stress close to the surface of the film. Meanwhile, the inner atoms are subjected to compressive stress due to the influence of implanted gallium ions. These two types of stresses occur within a thickness of ~20 nm on the top layer of the gold film, which further drives the elastic deformation of bottom layer. These cascaded displacements caused by knock-on events introduce complicated stresses and strains across the film (defined as $\sigma^{in-plane}$). Specifically, the residual stress distribution can be simplified into a bilayer stress model[2]

$$\sigma^{in-plane}(x_3) = \begin{cases} \sigma_t = const, \ \ h_b < x_3 \le h_b + h_t \\ \sigma_b = \sigma_0^{in-plane} + kx_3 + o(x_3), \ \ 0 \le x_3 \le h_b \end{cases} \quad (1)$$

Here, x_3 is the coordinate in the thickness direction; h_t and h_b are the thicknesses of top and bottom layers, respectively; σ_t and σ_b are the residual stress in the top and bottom layers, respectively; $\sigma_0^{in-plane}$ and k are the first- and second-order coefficient in the asymptotic expansion of stress in the bottom layer, with little $o(x_3)$ representing the higher orders (the higher-order term is negligible considering the ultrasmall thickness of the films). With such a residual stress distribution, the fabricated nano-kirigami structures are well reproduced by the numerical calculations, verifying the accuracy of the bilayer stress model. And meanwhile, the excellent consistence between experiments and calculations proves that, in the proposed nano-kirigami, the resulting structures are well predictable by the mechanical model. The simulation results of the bilayer stress model can provide the stress distribution inside the structure, the deformation height, etc., which provide an effective reference for the optimized design of the structure. Following this design principle, the kissing-loop nano-kirigami deformation results in Figures 1b-c are well generated by the numerical calculations. By setting two types of stress distributed on the gold film during the calculation, the deformation of the structure from 2D to 3D can be controlled, thus obtaining the desired structure.

Figure S2

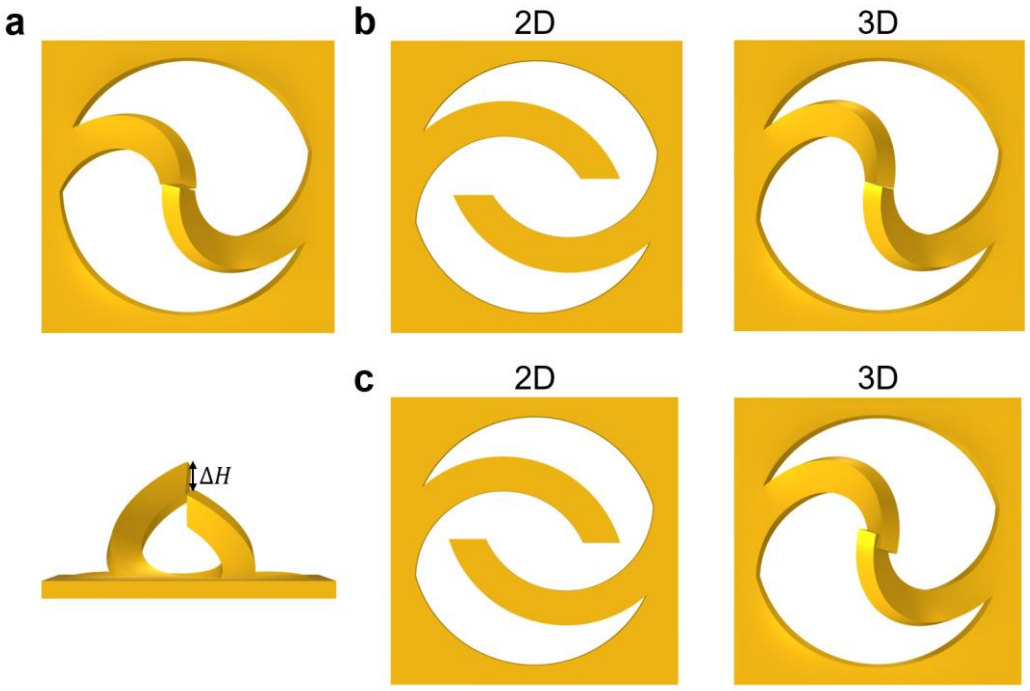

Figure S2. a) The top view and side view of kissing-loop nano-kirigami structure with different deformation heights ΔH between two cantilevers. b) The ideal kissing-loop nano-kirigami structure. c) The arm length of the cantilevers is designed larger than the ideal case so that there is a definite cross point in the upward deformation pathway.

Figure S3

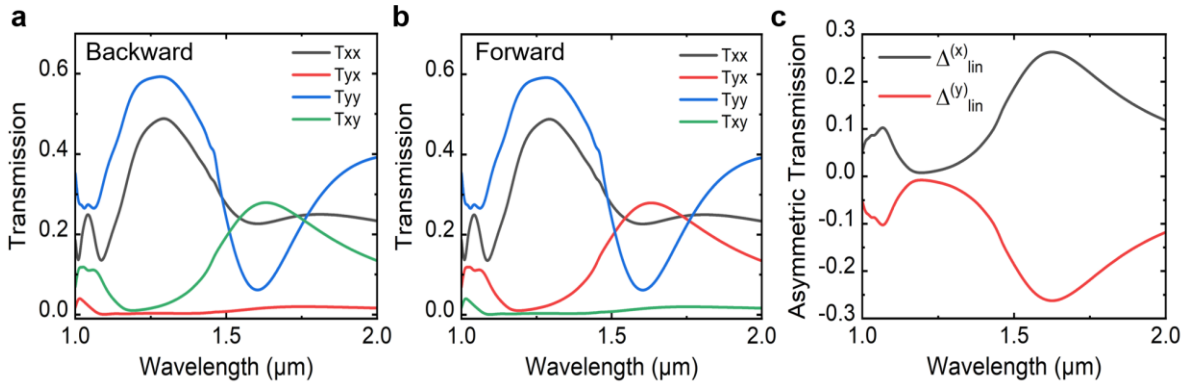

Figure S3. The simulated transmission spectra of 3D kissing-loop nano-kirigami strucutres for incident wave along the (a) backward and (b) forward directions. c) The simulated asymmetric transmission parameters of *x*- and *y*-polarized waves, respectively.

Figure S4

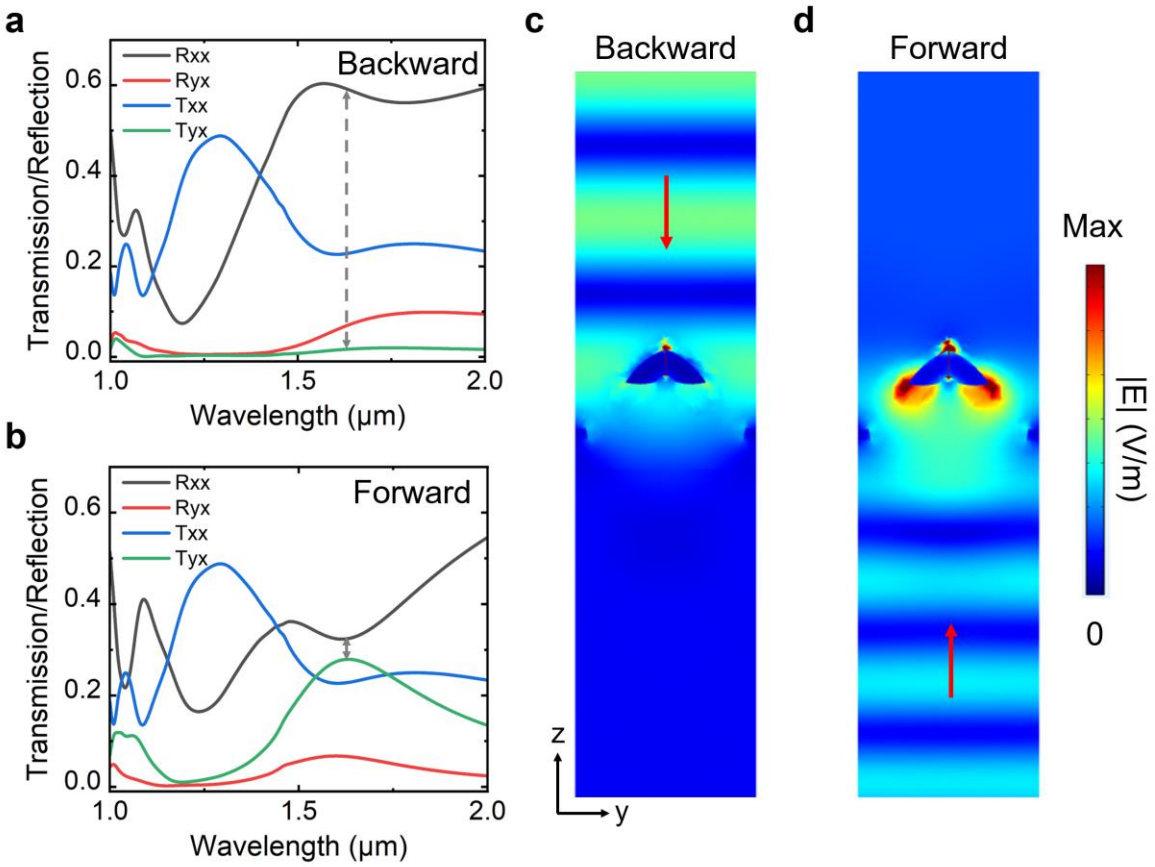

Figure S4. Analysis of asymmetric transmission of 3D kissing-loop nano-kirigami structures. a-b) The simulated reflection/transmission spectra for *x*-polarized wave incident along the backward and forward directions, respectively. The co-polarized reflection is strong and the cross-polarized transmission is only 0.02 under backward incidence, while the co-polarized reflection significantly decreases and the cross-polarized transmission increases to 0.28 under forward incidence, as marked by the gray arrows in Figures S4a-b. c-d) The electric field intensity distributions in the *y*-*z* plane at λ = 1.63 μm under backward and forward incidence, respectively. Figure S4c shows that there is a weak resonance induced by the kissing-loop nano-kirigami structure for *x*-polarized backward incidence, resulting in most of the incident light is reflected. Meanwhile, Figure S4d shows that, when *x*-polarized wave along forward incidence, a strong resonance mode is induced in two cantilevers, and thus the *x*-polarized incident light is transformed to *y*-polarized transmission.

Figure S5

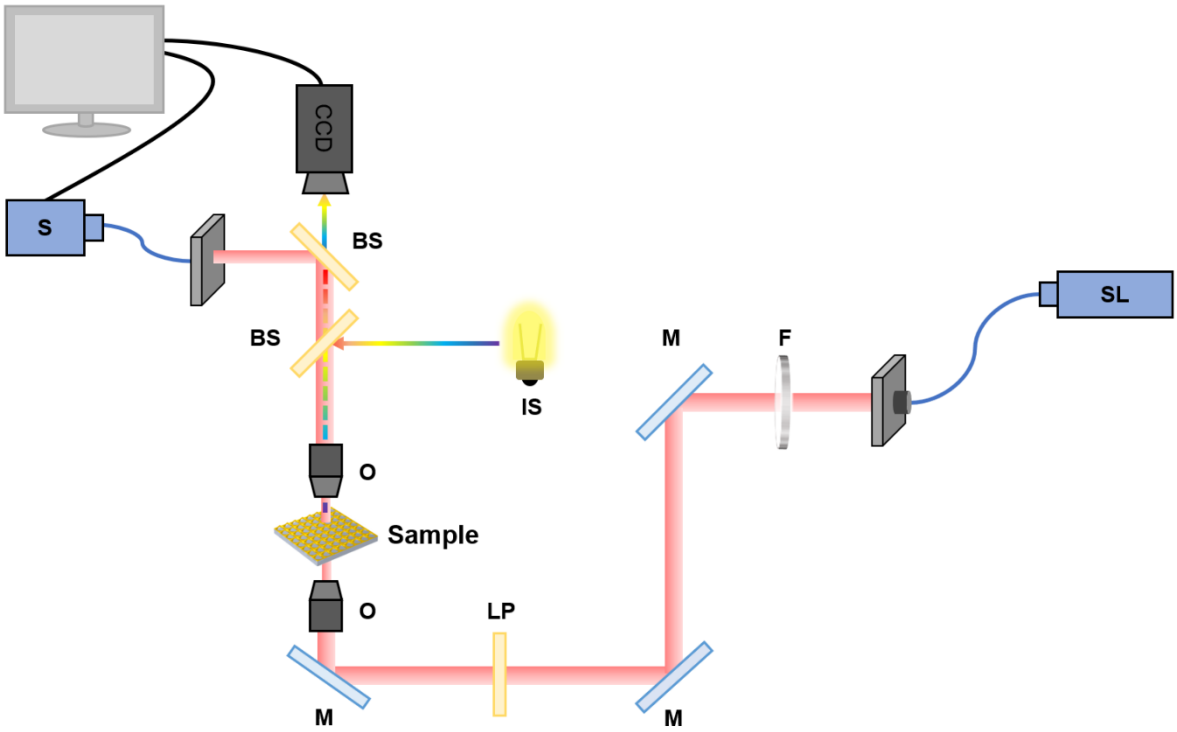

Figure S5. The optical setup design for cross-polarized transmission measurement. SL, supercontinuum laser; LP, linear polarizer; M, mirror; S, spectrometer; IS, illuminating source; BS, beam splitter; F, filter; O, objective.

Figure S6

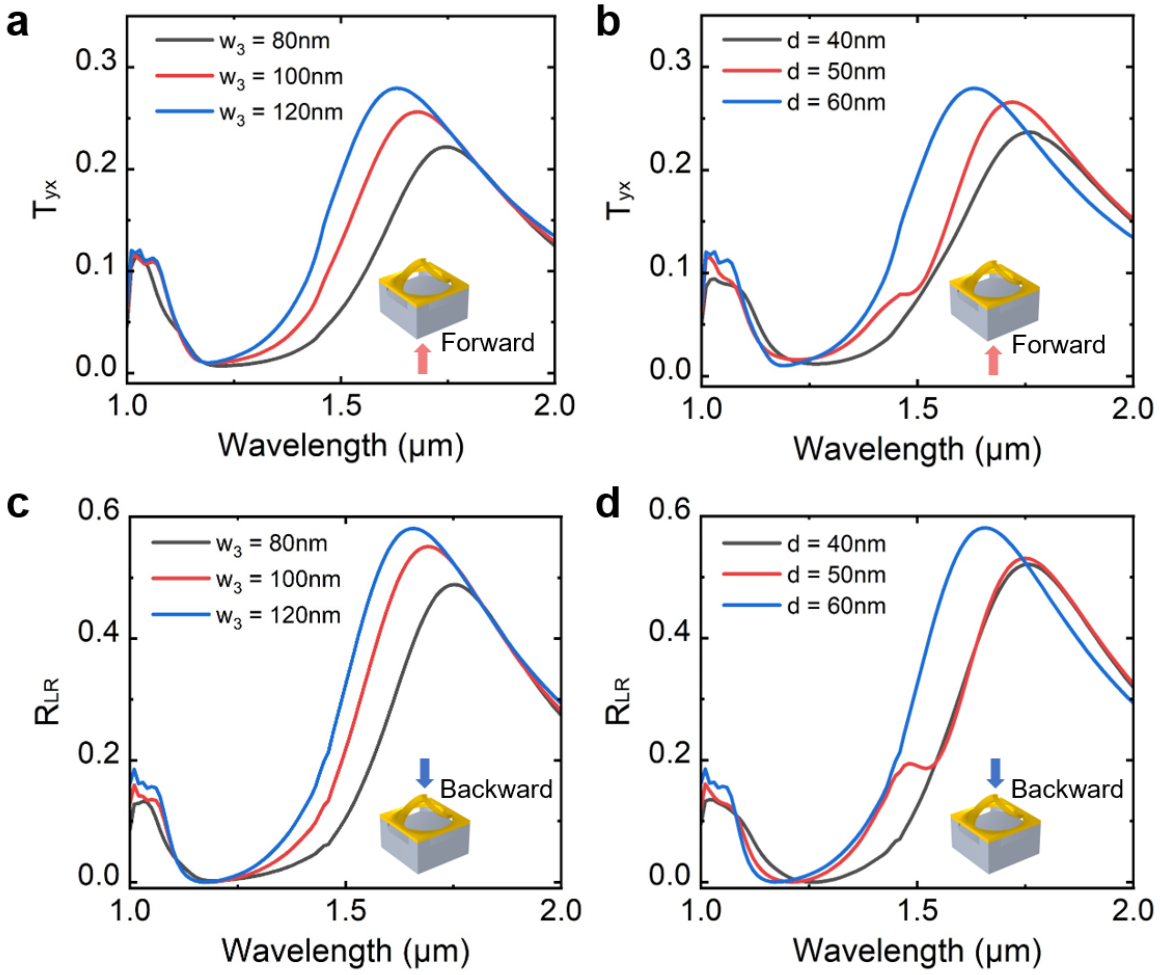

Figure S6. Effects of the width of cantilever and the thickness of gold film on optical properties of kissing-loop nano-kirigami structures. As (a) the width of cantilevers or (b) the thickness of the gold film decreases, the cross-polarized transmission T_{yx} of the kissing-loop nano-kirigami structures for *x*-polarized light incident along the forward direction decreases and the resonance peak red shifts. As (c) the width of cantilevers or (d) the thickness of the gold film decreases, the cross-polarized reflection R_{LR} of the kissing-loop nano-kirigami structures for RCP light incident along the backward direction decreases and the resonance peak is red shifted.

Figure S7

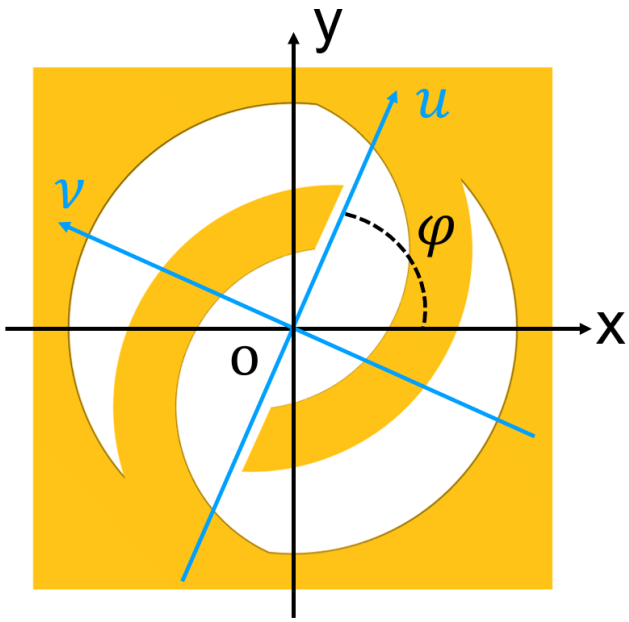

Figure S7. Local coordinate system of the structural unit.

Figure S8

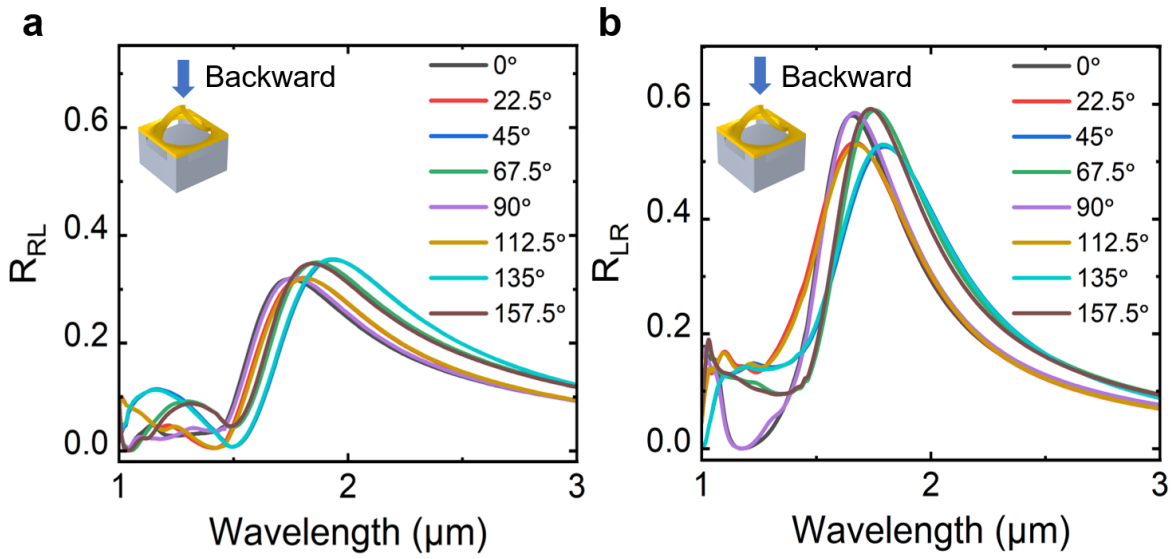

Figure S8. Simulated cross-polarized reflection spectra under (a) LCP and (b) RCP incidence for 3D kissing-loop nano-kirigami structures with various rotation angle φ. It can be seen that the cross-polarized reflections change a little with the rotation angle of 3D kissing-loop nano-kirigami structure under LCP and RCP incidence. R_{LR} is the cross-polarized reflection efficiency under RCP light incident.

Figure S9

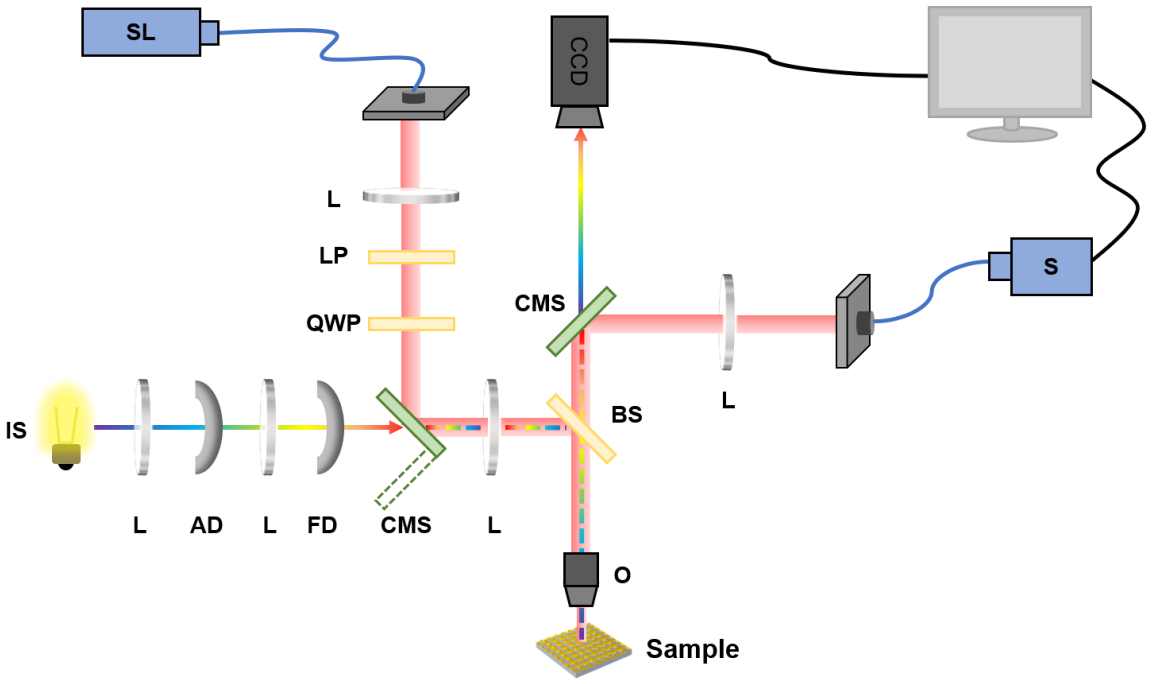

Figure S9. Schematic optical setup for the anomalous reflection experiment. SL, supercontinuum laser; LP, linear polarizer; QWP, quarter-wave plate; IS, illumination source; L, lens; AD, aperture diaphragm; FD, field diaphragm; CMS, optical path switcher; S, spectrometer; BS, beam splitter; O, objective.

References

1. Cui, A.; Liu, Z.; Li, J.; Shen, T. H.; Xia, X.; Li, Z.; Gong, Z.; Li, H.; Wang, B.; Li, J.; Yang, H.; Li, W.; Gu, C., Directly patterned substrate-free plasmonic “nanograter” structures with unusual Fano resonances. *Light: Science & Applications* **2015,** *4* (7), e308-e308.

2. Liu, Z.; Du, H.; Li, J.; Lu, L.; Li, Z.-Y.; Fang, N. X., Nano-kirigami with giant optical chirality. *Science advances 4* (7), eaat4436.